Solid Freeform Fabrication 2017: Proceedings of the 28th Annual International Solid Freeform Fabrication Symposium – An Additive Manufacturing Conference
Reviewed Paper

INVESTIGATION OF BUILD STRATEGIES FOR A HYBRID MANUFACTURING PROCESS PROGRESS ON TI-6AL-4V

Lei Yan[a], Leon Hill[a], Joseph W Newkirk[b], Frank Liou[a]
[a] Department of Mechanical and Aerospace Engineering
[b] Department of Materials Science and Engineering
Missouri University of Science and Technology, Rolla, MO

Abstract

The various processing parameters of a hybrid manufacturing process, including deposition and machining, is being investigated with a Design of Experiment (DoE). The intent was to explore the effect of different build strategies on the final part's Vickers hardness, tensile test, fatigue life, and microstructure. From this experiment, the processing parameters can be linked to various mechanical properties. This will lead to the ability to create a combination of deposition and machining parameters, which will result in improved mechanical properties.

Introduction

Laser metal deposition (LMD) has made many breaking through successes in complex parts manufacturing and new materials developing [1, 2, 3, 4]. However, due to the inherent rapid solidification property of LMD process, inevitable porosity, distortion, and rough surface finish of LMD build parts usually require post heat treatment and machining to meet end-use dimensional and mechanical requirements [5, 6, 7]. In addition, LMD manufactured parts are still non-comparable to conventional manufacturing methods in cost and productivity [6].

Hybrid manufacturing (HM) combines the freedom of additive with precision of computer numerical control (CNC) to enable done-in-one ability, which allows in-process quality inspection, speeds up production of complex metal parts, and overcomes the difficulty in machining inner features. In recent years, several HM systems have been developed, SLS/SLM with milling [7], arc welding with milling [8, 9, 10, 11], and machining center with LENS® function. However, few of them systematically investigated how HM processing parameters affect final product's mechanical properties and microstructure evolution. In this paper, a design of experiment (DoE) matrix was generated which includes primary processing parameters of deposition and machining process as input factors and microstructure, Vickers hardness, fatigue life, and tensile test results as responses. Herein, the main efforts were put on the investigation of appropriate ranges for the DoE input factors.

Experimental Procedures

All experiments were performed on a LMD system and a 5 axis FADAL CNC machine. The LMD system consists of a 1 kW solid-state YAG-fiber laser, a 3-axis CNC platform, an argon purged chamber, and a vertical powder delivery subsystem. Fig. 1a shows the schematic of the LMD system, where the laser beam diameter was set to 2 mm. Powders used in this research are gas atomized Ti-6Al-4V powder with mesh size -100/+325.

The illustration of the HM process is demonstrated in Fig. 1b, where end milling is applied between each deposition. A certain height of non-machined as-deposit surface, as-called shielding

height, is left to protect machined surface from spoiled by the following deposition process. The deposit height in between each machining process is called layer thickness. Each time the removed material thickness at each side is called depth of cutting, and usually several times cutting are needed to get required final thickness.

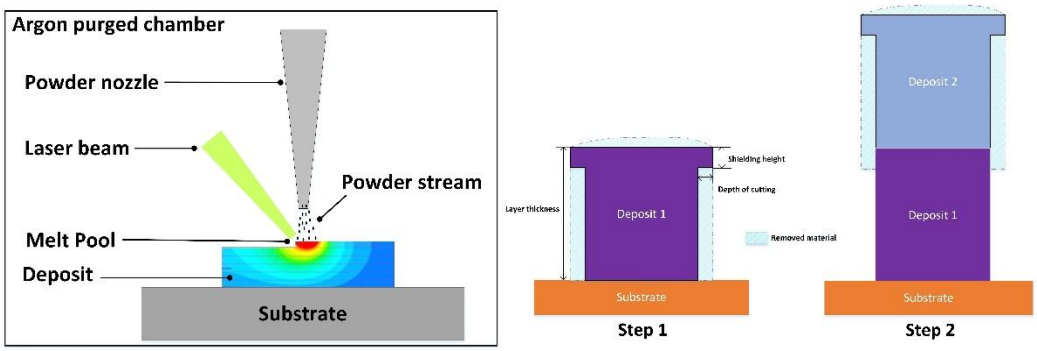

(a)LMD process (b)HM process

Figure 1: Schematic of the LMD and HM process

To explore the effects of different build strategies on the final part's properties, DoE matrix was implemented for a build which used multiple applications of deposition and machining, to make 30 mm tall and 2 mm thick thin- wall structures. Five parameters, layer thickness, depth of cutting, shielding height, preheating temperature, and laser energy density (LED) were selected for a set of screening DoE. Considering the accuracy and time efficiency, a five-factor two-level half-fractional DoE matrix was designed, consisting of $2^{5-1} = 16$ runs (resolution V design).

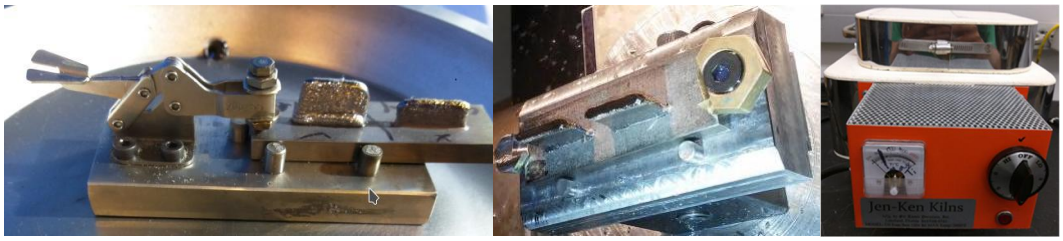

(a)AM fixture (b)machining fixture (c) Jen-Ken Kilns

Figure 2: fixtures used in the HM process

The low-level value (-1) and high-level value (+1) of the considered parameters are important to the whole experiment for which determines the applicable range of the analysis of variance (ANOVA) test results be applied to. Preliminary research was conducted to explore the maximum height increment per track that yields a stable buildup with maximum powder capture efficiency for each DoE run and 0.4 mm was the final selection. To reduce residual stress magnitudes and warping, uniform preheating of the substrate and deposit before each new deposition was considered [12]. When preheating applied, Jen-Ken Kilns, as shown in Fig. 2 (c) was used to heat substrate up to 573 K, where the oxygen weight gain is only 1.6 mg/cm2 and beyond which the value increases dramatically [13]. From measurements of as-deposit thin-wall structures, the thickness of them is around 4 mm at selected LED levels, which guaranteed to build full dense parts. In the machining process, both side surfaces and the top surface have been end milled with a 0.5" diameter tool at parameters: 275 surface feet/min, 0.0012 chip load, depth of cutting 0.05" to 0.1" for top surface, and 0.005" to 0.02" for side surface [14]. For layer thickness, 10 mm and 15 mm was selected as the low-level value and high-level value separately. Those two

height values are easy to get and high enough for small scale model analysis with DoE. The non-spoiled machined surface height has a linear relationship with depth of cutting and shielding height [15], based on the depth of cutting of each side surface, shielding height low-level and high-level was set to 1.2 mm and 2.2 mm.

Alignment between multiple deposition and machining system transitions during the HM process is critical and necessitated two sets of fixtures be designed to solve this issue. As shown in Fig. 2 (a) and (b), pins and clamps were used to guarantee alignment during each transition.

Experimental Results and Discussions

The LED is defined as$LED = P/v$, where P is laser power and v is laser traverse speed. LED is critical to microstructure evolution during LMD process then affects the final parts' mechanical properties. A finite element analysis (FEA) simulation of the LMD process was conducted to help selecting appropriate LED levels to avoid lack of fusion and overheat. An improvement was made to a previous work [2] and brings the FEA model closer to real world, where a heat sink was added to the left side of the substrate to simulate the fixture effect, which means fixture extracted heat is considered during heating and cooling.

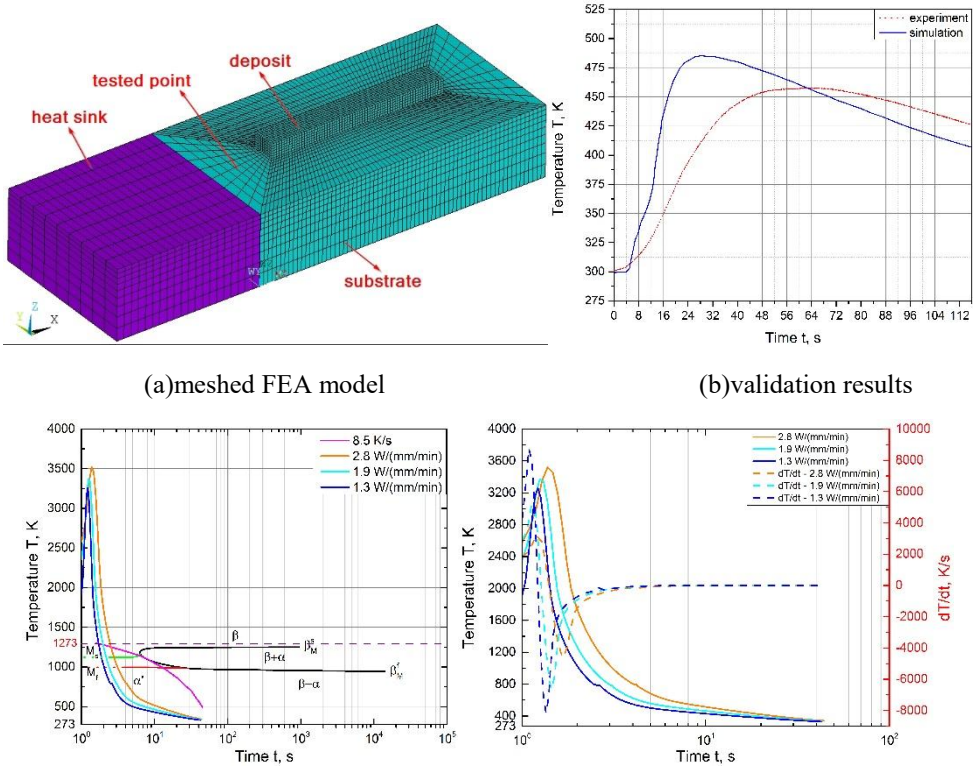

(a)meshed FEA model (b)validation results

(c)cooling curves with CCT diagram (d)cooling rate for 3 different cases

Figure 3: FEA simulation of the deposition process

To validate the new FEA model, a short deposition was ran and simulated with the exact LMD processing parameters. Fig. 3a shows the meshed FEA model with the heat sink and Fig. 3b shows the temperature comparison between simulation and experiment, where simulation result is close to the experiment one and there is only 25 K difference between the two temperature peaks. In the temperature measuring experiment, a K-type thermal couple was fixed to a shallow hole on

the substrate top surface with thermal paste cement, which may have had some thermal paste cement in between of the thermal couple tip and substrate and caused the thermal couple not to contact with the substrate directly. The low thermal conductivity of the thermal paste cement caused the experiment peak temperature lagging the simulated one. Also, thermal paste cement acts like insulation and makes resistance to cooling, which reflects in Fig. 3b is the experiment cooling rate value is higher than the simulated one. Before simulating the deposition part of the proposed HM process, an initial assumption of the minimum energy needed to melt introduced powders from the nozzle was conducted based on $Q = m * \Delta T * C_p$ and the latent heat of fusion$L$, where m denotes mass of the melted powders, ΔT is set as the powder temperature change from ambient temperature 300 K to melting point 1933 K, $C_p$is the specific heat. The energy efficiency of the LMD process with YAG laser is proved to be only 20% to 10% of the raw power be used to melt the powders [16]. Take laser traverse speed as 600 mm/min for example, the minimum laser power needed is 590 W and the LED is 0.98 W/(mm/min). With trial and error in real deposition experiment, minimum LED needed in our LMD system to build full dense part is 1.1 W/(mm/min), and 3 W/(mm/min) would cause severe overheat. In the FEA model, three cases were investigated with different LED level, 2.8 W/(mm/min) (2.8-LED), 1.9 W/(mm/min) (1.9-LED), and 1.3 W/(mm/min) (1.3-LED), respectively. In all the three cases investigated here, the first two tracks were deposited with 800 W laser power to generate molten pool, and the following tracks with laser power at 400 W. The LED was modified by adjusting laser traverse speed. For 1.9-LED level the laser traverse speed was set to 216 mm/min, 1.3-LED level 305 mm/min, and 2.8- LED level 143 mm/min. The phase fraction and microstructure size, which relies on the cooling rate, has direct effects on Vickers hardness and other mechanical properties of the final part. Cooling rate of the middle point in the very top layer was investigated at various LED level and plot in Fig. 3c combined with a simplified continuous cooling transformation (CCT) diagram. In Fig. 3c, time starts from laser hit the specific point and it could be seen that overheat occurs at 2.8-LED level and was observed in the experiment that half of the deposit was in red. For 1.9-LED and 1.3-LED levels, no overheat situation was found and scanning electron microscopy (SEM) of the deposit cross-section revealed full dense part and no porosity, indicating sufficient LED input. So, the LED low-level and high-level value was set to 1.3-LED and 1.9-LED. In Fig. 3d, it can be found that the higher the LED level the lower the cooling rate at the beginning, which caused by larger energy input results in more heat accumulated in the structure that leads the whole structure takes more time to disperse heat to surroundings. After a certain time, the cooling rate for different LED levels tends to get close as heat has been extracted to substrate and clamping fixture that causes heat conduction become slowly.

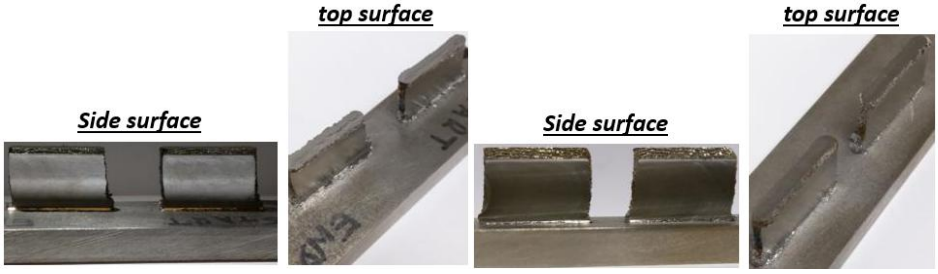

(a)1.9-LED machined surfaces (b) 1.3-LED machined surfaces

Figure 4: machined surfaces of the two different LED cases

To validate the LED low-level and high-level selection, deposits built at those two LED levels were machined and the surface integrity of the machined surfaces was compared, as shown in Fig. 4 where non-oxidized and well bounded Ti-6Al-4V thin-wall structures were machined on two laser traverse directional side surfaces and top surface. Optical microscopy was utilized to analyze the 3D profile of the machined surfaces and the analysis results are shown in Fig. 5, where black line indicates surface profile, red line indicates roughness, and green line indicates waviness. It can be found that in both 1.3-LED and 1.9-LED level cases, the side surface has a better roughness value than the top surface, and the machined surfaces in 1.3-LED case has a better roughness value than in 1.9-LED case. Based on the analysis of the FEA simulation results, higher laser traverse speed means lower LED input, which tends to have higher cooling rate [17]. As we can see in Fig. 3c, high cooling rate would benefit for finer grains and martensitic-α forming. Finer grains and high-volume fraction of martensitic-α in the final part built by 1.3-LED level leads to a higher Vickers hardness which causes the part harder for machining at the same machining condition compare to 1.9-LED level case, which results in a rougher surface integrity.

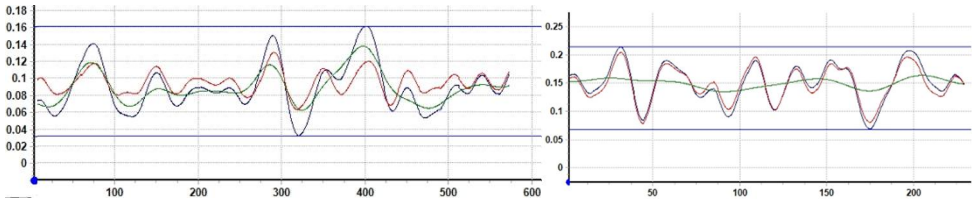

(a)1.9-LED top surface integrity (b)1.3-LED top surface integrity

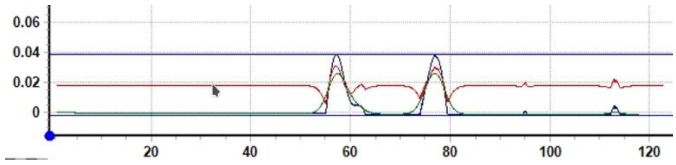

(c)1.9-LED side surface integrity

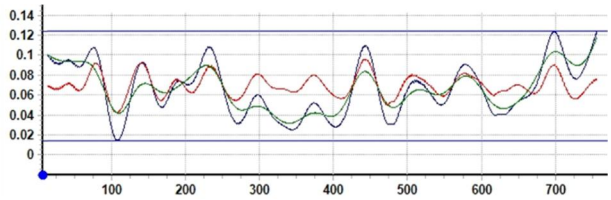

(d) 1.3-LED side surface integrity

Figure 5: surface integrity of two different LED cases

The final low-level and high-level values of each factor is given in Table 1 and the designed matrix is in Table 2. Based on the normalized orthogonal matrix, the factorial DoE represents various processing conditions and ensures the effect of each factor can be clearly evaluated.

Table 1: ranges of the investigated HM processing parameters

Label	Parameters	Low-level (-1)	High-level (+)
A	Layer thickness	10 mm	15 mm
B	Depth of cutting	0.5 mm	1 mm
C	Preheating temperature	300 K	573 K
D	Shielding height	1.2 mm	2.2 mm
E	Laser energy density	1.3 W/(mm/min)	1.9 W/(mm/min)

Table 2: DoE matrix

Run	A	B	C	D	E	Treatment combination
1	-	-	-	-	+	e
2	+	-	-	-	-	a
3	-	+	-	-	-	b
4	+	+	-	-	+	abe
5	-	-	+	-	-	c
6	+	-	+	-	+	ace
7	-	+	+	-	+	bce
8	+	+	+	-	-	abc
9	-	-	-	+	-	d
10	+	-	-	+	+	ade
11	-	+	-	+	+	bde
12	+	+	-	+	-	abd
13	-	-	+	+	+	cde
14	+	-	+	+	-	acd
15	-	+	+	+	-	bcd
16	+	+	+	+	+	abcde

Conclusion

A five-factor two-level half-fractional DoE matrix has been successfully developed with appropriate low-level and high-level values for each factor. LED range selection was especially investigated with a high accuracy validated FEA model, which will benefit cost reduction in both time and material in future for complex shape parts developing with HM process.

In future, thin-wall structures will be built according to the DoE matrix and the Vickers hardness, fatigue, and tensile tests will be applied and analyzed with the ANOVA test. An optimized build strategy can be generated from the ANOVA analysis results.

Acknowledgment

This project was supported by The Boeing Company through the Center for Aerospace Manufacturing Technologies (CAMT), National Science Foundation Grant #CMMI-1547042, and the Intelligent Systems Center (ISC) at Missouri S&T. Their financial support is greatly appreciated.

References

[1] W. Li, L. Yan, S. Karnati, F. Liou, J. Newkirk, K. M. B. Taminger, W. J. Seufzer, Ti-fe intermetallics analysis and control in joining titanium alloy and stainless steel by laser metal deposition, Journal of Materials Processing Technology 242 (2017) 39-48.

[2] L. Yan, W. Li, X. Chen, Y. Zhang, J. Newkirk, F. Liou, D. Dietrich, Simulation of cooling rate effects on ti-48al-2cr-2nb crack formation in direct laser deposition, JOM (2016) 1-6.

[3] L. Yan, X. Chen, W. Li, J. Newkirk, F. Liou, Direct laser deposition of ti-6al-4v from elemental powder blends, Rapid Prototyping Journal 22 (2016) 810-816.

[4] L. D. Bobbio, R. A. Otis, J. P. Borgonia, R. P. Dillon, A. A. Shapiro, Z.-K. Liu, A. M. Beese, Additive manufacturing of a functionally graded material from ti-6al-4v to invar: Experimental characterization and thermodynamic calculations, Acta Materialia (2017).

[5] D. Homar, F. Pusavec, The development of a recognition geometry algorithm for hybrid-subtractive and additive manufacturing, Strojniski vestnik-Journal of Mechanical Engineering 63 (2017) 151-160.

[6] T. Yamazaki, Development of a hybrid multi-tasking machine tool: Integration of additive manufacturing technology with cnc machining, Procedia CIRP 42 (2016) 81-86.

[7] Z.-p. Ye, Z.-j. Zhang, X. Jin, M.-Z. Xiao, J.-z. Su, Study of hybrid additive manufacturing based on pulse laser wire depositing and milling, The International Journal of Advanced Manufacturing Technology (2016) 1¬12.

[8] X. Xiong, H. Zhang, G. Wang, Metal direct prototyping by using hybrid plasma deposition and milling, journal of materials processing technology 209 (2009) 124-130.

[9] X. Xiong, Z. Haiou, W. Guilan, A new method of direct metal prototyping: hybrid plasma deposition and milling, Rapid Prototyping Journal 14 (2008) 53-56.

[10] Y.-A. Song, S. Park, Experimental investigations into rapid prototyping of composites by novel hybrid deposition process, Journal of Materials Processing Technology 171 (2006) 35-40.

[11] K. Karunakaran, S. Suryakumar, V. Pushpa, S. Akula, Retrofitment of a cnc machine for hybrid layered manufacturing, The International Journal of Advanced Manufacturing Technology 45 (2009) 690-703.

[12] A. Vasinonta, J. Beuth, M. Griffith, Process maps for laser deposition of thin-walled structures, in: Solid Freeform Fabrication Proceedings, The University of Texas at Austin, August, pp. 383-391.

[13] E. Gemelli, N. Camargo, Oxidation kinetics of commercially pure titanium, Materia (Rio de Janeiro) 12 (2007) 525-531.

[14] S. Vijay, V. Krishnaraj, Machining parameters optimization in end milling of ti-6al-4v, Procedia Engineering 64 (2013) 1079-1088.

[15] T. A. Amine, T. E. Sparks, F. Liou, A strategy for fabricating complex structures via a hybrid manufacturing process, in: 22nd Annual International Solid Freeform Fabrication Symposium An Additive Manufacturing Conference, SFF, pp. 175-184.

[16] K. Salonitis, L. DAlvise, B. Schoinochoritis, D. Chantzis, Additive manufacturing and post-processing simulation: laser cladding followed by high speed machining, The International Journal of Advanced Manufacturing Technology 85 (2016) 2401-2411.

[17] L. Wang, S. Felicelli, Y. Gooroochurn, P. Wang, M. Horstemeyer, Optimization of the lens® process for steady molten pool size, Materials Science and Engineering: A 474 (2008) 148-156